HHS Public Access

Author manuscript

Magn Reson Med. Author manuscript; available in PMC 2017 July 01.

Published in final edited form as:

Magn Reson Med. 2016 July ; 76(1): 118–126. doi:10.1002/mrm.25864.

TOWERS: T-One with Enhanced Robustness and Speed

Cihat Eldeniz[1], **Jürgen Finsterbusch**[2], **Weili Lin**[1], and **Hongyu An**[1,*]

[1]Department of Radiology, University of North Carolina at Chapel Hill

[2]Department of Systems Neuroscience, University Medical Center, Hamburg-Eppendorf

Abstract

Purpose—A new T1 mapping method is proposed that is accurate, rapid and robust to motion. Considering these features, the method is dubbed "T-One with Enhanced Robustness and Speed (TOWERS)".

Methods—TOWERS is composed of inversion recovery (IR) and saturation recovery (SR) acquisitions. In the IR acquisitions, a slice reordering scheme is employed in order to sample all slices in an efficient manner, whereas the SR acquisitions serve as references for motion estimation. Furthermore, as opposed to the usual way of running GRAPPA calibration only once at the beginning, GRAPPA coefficients are updated in the middle and at the end, and are later used for retrospectively correcting for motion artifacts. Finally, sub-voxel magnetization tracking is deployed to account for motion-induced signal evolution changes.

Results—Whole-brain T1 mapping data with a spatial resolution of 1.56 × 1.56 × 2.00 mm can be collected within 2.5 minutes. TOWERS and the gold-standard IR method agree well in phantom, while high reproducibility is achieved in vivo. High-quality T1 maps in the presence of severe motion show the robustness of the method.

Conclusion—The proposed method, TOWERS, is shown to be rapid, accurate and robust. Multiple GRAPPA calibrations and sub-voxel magnetization tracking make TOWERS unique.

Keywords

MRI; GRAPPA; EPI; Fast T1 Mapping; Robustness to Motion; Magnetization Tracking

Introduction

In MR imaging, the longitudinal relaxation time, T1, is one of the most fundamental parameters and provides the basis for superior soft tissue contrast. Quantitative T1 measurement is thus vital for many MR applications such as blood-brain barrier permeability measurements (1–3), quantitative arterial spin labeling computation (4,5), temperature mapping (6–8), and tissue suppression (9,10).

Numerous T1 mapping methods have been proposed to date. Among these methods, the inversion recovery (IR) sequence (11) remains the gold standard, due to the fact that it

*Corresponding author: Hongyu An, hongyu_an@med.unc.edu, Phone: 001-919-843-8256.

provides the highest possible dynamic range for T1 recovery. In a conventional IR sequence, an idle time interval, termed as the inversion time (TI), is placed between the inversion pulse and the data acquisition block. Multiple measurements with various TI values are needed in order to measure T1 accurately. After each measurement, the system is left idle in order to restore the longitudinal magnetization back to equilibrium. Because of the wait times before and after each measurement, the IR method suffers from a substantially long acquisition time, which limits its use in vivo. Progressive saturation (PS) sequence (12) is a faster option, but, since no inversion pulses are played, the dynamic range is small, making the sequence prone to noise. The variable flip angle (VFA) method (13) is another fast alternative; however, in the presence of B1-field inhomogeneities which are particularly exacerbated for high and ultra-high field MR, the flip angles can deviate significantly from the assumed values. The Look-Locker (LL) method and its variants (14–17) collect multiple samples per single inversion event. These methods are fast, but the collected samples are noisy due to the use of low flip angles. Furthermore, the dynamic range is narrow due to the perturbation of magnetization by the application of a train of RF pulses.

Another class of rapid sequences makes use of slice reordering (18–20). The slices of interest are inverted in groups and then sampled in an order that is circularly-shifted from repetition to repetition. This scheme makes it possible to rapidly obtain a sufficiently high number of TIs for all slices.

To the best of our knowledge, no T1 mapping study to date has specifically dealt with motion. If the subject moves during the acquisition of any of the aforementioned sequences, either the data up until the time of motion needs to be used, if at all possible, or the whole measurement needs to be repeated.

To this end, we sought to develop a rapid, accurate and robust whole-brain T1 quantification method. We name the new sequence as TOWERS – T-One With Enhanced Robustness and Speed (21). We have evaluated the accuracy of TOWERS against the gold-standard IR method in phantom. The reproducibility of the method and the robustness to motion have also been assessed in normal subjects.

Methods

Slice reordering

T1 is typically measured by sampling the inversion recovery process at different points in time. The acquisition begins with an inversion pulse. After a certain TI, an excitation pulse is applied to rotate the longitudinal magnetization into the transverse plane for signal read-out. This procedure needs to be repeated several times, each time with a different TI, in order to obtain an adequate sampling of the T1 recovery process. The main disadvantage of this scheme is that it is extremely time-inefficient because of the long wait times.

As a remedy, a high-speed multislice scheme was previously proposed (18). In this scheme, the slices were circularly permuted from repetition to repetition. Consequently, for an N-slice acquisition, N samples were obtained for each slice at the end of N repetitions. Similar schemes were proposed that circularly shifted slices by 1 slice at a time within the slabs of a

volume (19), or by 2 slices at a time within the whole volume, reducing the number of repetitions by a factor of 2 and hence trading precision for speed (20).

Despite their effective use of time, the slice-shifting methods mentioned thus far suffer from the same short-coming: if motion occurs early in the scan, it will be very difficult to obtain good-quality T1 estimates due to the substantially reduced number of samples. Perhaps, a reacquisition will be necessary. In this respect, the proposed scheme, TOWERS, consists of two acquisition periods, each of which can be used independently for computing a T1 map. Together with the application of an adiabatic non-selective inversion pulse, the slices are circularly shifted by 4 slices at a time across repetitions within each acquisition period, with a shift of 2 slices between the periods. This way, the slices will have been effectively shifted by 2 slices at a time. Figure 1 depicts the two-period acquisition scheme.

Saturation recovery (SR) samples

In an IR repetition where a non-selective inversion pulse is played, the slices manifest different contrast depending on when they are sampled during recovery. Considering the fact that the slices are circularly shifted from repetition to repetition, the intravolume contrast pattern will be different at each repetition, making it difficult to perform intervolume registration across repetitions. In an SR repetition, however, no inversion pulses are applied. The SR repetitions therefore enjoy a consistent intravolume contrast pattern, no matter when they are acquired within the sequence. This makes it possible to perform intervolume registration between the SR samples and thus estimate the motion between the acquisition periods, if any.

GRAPPA calibration

Generalized Autocalibrating Partially Parallel Acquisitions (GRAPPA) (22) is a well-accepted and widely-used parallel imaging technique that aims at reducing the acquisition time by subsampling the k-space. The missing lines are filled out by a weighted sum of the acquired lines, where the weights are calculated by means of a calibration scan that is typically performed at the very beginning of image acquisition. However, in the case of motion, the weights become invalid and can lead to substantial ghosting. In this regard, we developed an in-house program to implement two additional calibration scans into the sequence that update the weight set – one before the second acquisition period and one at the very end. The very last calibration is useful in that it is performed at the final position of the subject. The weight set calculated for this calibration can be applied retrospectively to its preceding repetitions in order to minimize the effects of motion in those repetitions.

Overall acquisition scheme

Figure 2 demonstrates the overall acquisition scheme. Benefiting from the SR repetitions and the attached calibration scans, the sequence can accommodate three different positions rather than assuming that the subject remains still throughout the whole acquisition.

Efficiency figure of merit

In order to demonstrate the high throughput of TOWERS, we define a figure of merit for efficiency:

$$\eta = \frac{\text{Number of Slices} \times \text{Number of Samples Collected Per Voxel}}{\text{Total Acquisition Time}} \quad [1]$$

Estimating T1 in the absence of motion

For an initial longitudinal magnetization value of $M_{z'}(0) = M_{z',0}$, the T1 relaxation can be expressed as:

$$M_{z'}(t) = M_{z',0}e^{-t/T_1} + M_o(1 - e^{-t/T_1}) \quad [2]$$

where M_o is the equilibrium magnetization. When a slice-selective 90-degree excitation pulse is applied to a slice, the longitudinal magnetization is nullified for all of the spins on that slice and it will start to recover from $M_{z'}(0) = 0$, in which case:

$$M_{z'}(t) = M_o(1 - e^{-t/T_1}) \quad [3]$$

which is basically the equation for saturation recovery. Since no inversion pulses are played during the GRAPPA calibration repetitions and the SR repetitions, any given slice has one full repetition to relax before being sampled at the SR repetition. It is worth noting that this whole-TR relaxation increases the dynamic range of the acquisition. The magnetization sampled at the GRAPPA calibration and SR repetitions can be expressed as:

$$M_{z',s,r}(M_o, T_1) = M_o(1 - e^{-TR/T_1}) \quad [4]$$

where s is the slice index, r is the repetition index, TR is the repetition time. It can be seen that the magnetization is independent of s and r.

On the other hand, in the IR repetitions, the longitudinal magnetization of Slice s at Repetition r will have the following initial condition right after the application of the inversion pulse:

$$M_{z',0,s,r}(M_o, T_1) = -M_o\left(1 - e^{-(TR - TI_{s,r-1})/T_1}\right) \quad [5]$$

where $TI_{s,r-1}$ is the inversion time for Slice s at Repetition $(r-1)$, and $(TR - TI_{s,r-1})$ is the time interval within which the spins on Slice s relax before the application of the inversion pulse at Repetition r. The minus sign in front of M_o is due to inversion. The spins will now relax with this initial magnetization until Slice s is sampled at the current repetition. The longitudinal magnetization right before this sampling event can be expressed as:

$$M_{z',s,r}(M_o,T_1)=M_{z',0,s,r}e^{-TI_{s,r}/T_1}+M_o\left(1-e^{-TI_{s,r}/T_1}\right)$$
$$=-M_o\left(1-e^{-(TR-TI_{s,r-1})/T_1}\right)e^{-TI_{s,r}/T_1}+M_o\left(1-e^{-TI_{s,r}/T_1}\right)$$
$$=M_o\left(1-2e^{-TI_{s,r}/T_1}\right)+M_oe^{-(TR+TI_{s,r}-TI_{s,r-1})/T_1} \quad [6]$$

where $TI_{s,r}$ is the inversion time for Slice s at Repetition r.

Eqs. [3]–[6] assume ideal RF pulses. That is, the excitation flip angle α=90° and the inversion flip angle β=180°. However, this is not true in practice – the actual values of these flip angles will depend on many factors and exhibit spatial variations. In this regard, the model equations need to be revised to accommodate these variations.

Due to the imperfection of the 90-degree excitation pulses, the spin history is never reset, which in turn makes the model equations recursive. We initialize the recursion by setting

$$M_{z'}=M_o \quad [7]$$

During the first dummy scan repetition, the imperfect excitation pulse leads to a residual longitudinal component that can be expressed as:

$$M_{z',0}=M_{z'}\cos(\alpha) \quad [8]$$

This residual longitudinal magnetization is going to experience T1-recovery until the application of the excitation pulse in the upcoming repetition, at which time it will become:

$$M_{z'}=M_{z'}(TR;M_o,T_1,\alpha)=M_{z',0}e^{-TR/T_1}+M_o\left(1-e^{-TR/T_1}\right) \quad [9]$$

For the rest of the dummy scan repetitions as well as for the GRAPPA calibration repetition, the left-hand-side (LHS) of Eq. [9] will be substituted into Eq. [8] and then the LHS of Eq. [8] will be substituted into Eq. [9] in order to arrive at the next value of $M_{z'}$each time.

At the first SR repetition (r = 1), the longitudinal magnetization $M_{z'}$obtained by Eq. [9] for the GRAPPA calibration repetition will be sampled by an excitation pulse, yielding:

$$M_{\perp,s,r}(M_o,T_1,\alpha)=M_{z'}(TR;M_o,T_1,\alpha)\sin(\alpha) \quad [10]$$

$$M_{z',0}=M_{z'}(TR;M_o,T_1,\alpha)\cos(\alpha) \quad [11]$$

where $M_{\perp,s,r}$ is the transverse magnetization to be measured by the receiver for Slice s and Repetition r. The initial longitudinal magnetization given in Eq. [11] is going to relax until the application of the inversion pulse at the first IR repetition. The wait time during which this relaxation occurs can be expressed as $t_w = (TR - TS_{s,r=1})$ where $TS_{s,r}$ is the saturation time for Slice s and Repetition r. The resulting longitudinal magnetization will become

$$M_{z'}=M_{z'0}e^{-t_w/T_1}+M_o\left(1-e^{-t_w/T_1}\right) \quad [12]$$

The application of the inversion pulse at the first IR repetition ($r = 2$) results in the following initial magnetization value for the relaxation that is going to take place until the application of the excitation pulse in that repetition:

$$M_{z',0}=M_{z'}\cos(\beta) \quad [13]$$

With this initial value, the longitudinal magnetization just before the application of the excitation pulse becomes:

$$M_{z'}=M_{z'}\left(TI_{s,r};M_o,T_1,\alpha,\beta\right)=M_{z',0}e^{-TI_{s,r}/T_1}+M_o\left(1-e^{-TI_{s,r}/T_1}\right) \quad [14]$$

The transverse and longitudinal magnetization after the application of the excitation pulse can be expressed as:

$$M_{\perp,s,r}(M_o,T_1,\alpha,\beta)=M_{z'}\left(TI_{s,r};M_o,T_1,\alpha,\beta\right)\sin(\alpha) \quad [15]$$

$$M_{z',0}=M_{z'}\left(TI_{s,r};M_o,T_1,\alpha,\beta\right)\cos(\alpha) \quad [16]$$

Derivation of the magnetization for all other repetitions is performed following the same flow of ideas. After calculating the transverse magnetization for all repetitions, the sum of squared residuals can be written as:

$$f_{x,y,s}(M_o,T_1,\alpha,\beta)=\sum_{r=1}^{N_r}\left[M_{\perp,s,r}(M_o,T_1,\alpha,\beta)-I_{x,y,s,r}\right]^2 \quad [17]$$

where N_r is the total number of repetitions and $I_{x,y,s,r}$ is the actual measurement for Voxel (x, y) of Slice s at Repetition r. Please note that, since the first SR measurement does not depend on β, $M_{\perp,s,r}(M_o, T_1, \alpha, \beta)$ should be considered constant in β for $r = 1$. (The other two SR measurements do depend on β because of the spin history). A least-squares fitting procedure that minimizes $f_{x,y,s}(M_o, T_1, \alpha, \beta)$ will then yield M_o, T_1, α and β for voxel (x, y) of Slice s.

It is worth noting that M_o and α are competing parameters that highly affect each other during fitting. The same is true for T_1 and β. For this reason, each iteration of the fitting procedure is performed in two steps. At the first step of the first iteration, M_o and β are estimated by choosing reasonable initial values for T_1 and α. At the second step, the estimates of M_o and β obtained at the first step are substituted into the model equation in order to estimate T_1 and α this time. Later, the estimates of T_1 and α are used for the first step of the second iteration and so on.

Although the increased number of parameters reduces the statistical power of the estimation, TOWERS offers a sufficiently high number of samples that are still able to yield high-quality estimates. As an example, a 60-slice acquisition collects 33 samples per voxel in order to estimate the 4 parameters of interest.

Motion detection

Since, in an IR repetition, the signal intensities can vary greatly across slices, the 5 highest-intensity slices are selected for motion detection. In order to simplify the illustration of the method, these five-slice bundles from each repetition will be termed as *High5*. Each of the slices in the High5 group of an IR repetition is compared to its counterpart in the most recent SR repetition via the following 2D cross-correlation metric:

$$\rho(s,r_i,r_s)=\frac{\Sigma_x\Sigma_y I(x,y,s,r_i)I(x,y,s,r_s)}{\sqrt{\Sigma_x\Sigma_y I(x,y,s,r_i)^2}\sqrt{\Sigma_x\Sigma_y I(x,y,s,r_s)^2}} s\in H_{5,r_i} \quad [18]$$

where s is the slice index, r_i is the IR repetition index, r_s is the SR repetition index and H_{5,r_i} is the set of High5 slices at Repetition r_i. If any of the comparisons yields a correlation value less than 95%, the motion detection scheme issues a warning and suggests the SR repetition index yielding the highest correlation as the index of the weight set to be used. The user checks the images as well as the suggestions by the motion detection scheme and makes the final decision as to which SR repetition a given IR repetition is associated with in terms of GRAPPA calibration. All of the repetitions are then reconstructed retrospectively with the assigned GRAPPA weight sets. Figure 3 illustrates this retrospective scheme.

Magnetization tracking

Motion disturbs the acquisition in two ways. The first problem is that, as mentioned above, the GRAPPA weights become invalid and this can lead to ghosting in the images. The second and the more serious problem is that the spins on the same slice can appear on different slices after motion. Figure 4 (a) illustrates this phenomenon. Voxel P gets relocated onto neighboring slices after each instance of motion. Since the order of acquisition is of utmost importance in our scheme, relocation of spins onto different slices severely corrupts the spin history. Figure 4 (b) shows the motion-free and motion-corrupted magnetization pathways for the spins that belong to Voxel P. This figure suggests that even a small displacement along the slice-select axis can lead to a substantial change in the magnetization pathway. Therefore, it is essential to track the location of spins in order to account for the effects of motion.

The tracking procedure begins by registering the second and the third SR images onto the first SR image using FSL's linear registration tool FLIRT (23,24). In addition to the registered image, FLIRT also outputs a 4×4 transformation matrix that encapsulates the rotation and translation parameters estimated during registration. We use this transformation matrix to map a point in the source image space to its corresponding point in the target image space. Once the trajectory of the spins in a voxel is determined, the overall magnetization pathway for the spins in that voxel can be fully described. In this respect, the derivations listed in Eqs. [7]–[17] need to go under two major modifications. The first modification is that s, the slice index, needs to be replaced with s_r where s_r indicates the slice on which the spins of interest appear at Repetition r. This modification provides flexibility – any given spin can now appear on different slices throughout the measurement. The second modification is that, as the positions of the spins change, α and β should also change because α and β are spatially varying as noted above. For instance, if the subject stays in 3 different positions during the scan, α and β will assume 3 different values and these need to appear in the model equations. In this case, the number of parameters to be estimated becomes 8.

It is worth noting that the motion-corrupted repetitions as well as the repetitions right after them need to be discarded, because the spin history becomes intractable at these repetitions.

The cost function will become:

$$f_{x,y,s}(M_o, T_1, \alpha_1, \beta_1, \ldots, \alpha_P, \beta_P) = \sum_{r \in R_u} \left[M_{\perp,s_r,r}(M_o, T_1, \alpha_1, \beta_1, \ldots, \alpha_P, \beta_P) - I_{x,y,s_r,r} \right]^2$$

[19]

with P being the number of different positions and R_u being the set of repetitions that are used during fitting and satisfying $|R_u| < N_r$.

Sub-voxel magnetization tracking

The estimation procedure described so far treats each voxel as a single fixed unit and tracks its trajectory accordingly. However, the spins in a given voxel may be redistributed into different voxels after motion. In this respect, it is more reasonable to represent each voxel as a 3D lattice of sub-voxel spin volumes. Let $N_{SVsPerDim}$ denote the number of spin volumes along a single dimension so that the total number of spin volumes in a given voxel will be given by $N_{SVs} = N_{SVsPerDim} \times N_{SVsPerDim} \times N_{SVsPerDim}$. When reconstructing the model equation for each individual spin volume, M_o will be replaced with M_o/N_{SVs}, while the T_1 value of each spin volume will be the same as the T_1 value of the original voxel.

As for the measurements to be used as the target during fitting, if Spin Volume k is found to fall into a voxel with intensity I after motion, the target value will be set to I/N_{SVs}. With the modeled and the target values at hand, the costs of all spin volumes will be summed up, and this sum will be minimized to arrive at the (M_o, T_1) pair for the voxel of interest that

originally encapsulated all these N_{SVs} spin volumes. In this respect, the cost function can be expressed as:

$$f_{x,y,s}(M_o, T_1, \alpha_1, \beta_1, \ldots, \alpha_P, \beta_P) = \sum_{k=1}^{N_{SVs}} \sum_{r \in R_u} \left[M_{\perp, s_r, r}\left(\frac{M_o}{N_{SVs}}, T_1, \alpha_1, \beta_1, \ldots, \alpha_P, \beta_P\right) - \frac{I_{x,y,s_r,r,k}}{N_{SVs}} \right]^2 \quad [20]$$

where *k*, being the spin volume index, signifies the fact that each spin volume has its own magnetization pathway.

Experiments

All experiments were run on a Siemens Tim Trio 3T MR scanner (Siemens Healthcare, Erlangen, Germany).

Four different concentrations of Ni(II)SO_4.6H_2O were prepared to mimic the T1 values encountered in the human brain. The approximate concentrations of the phantoms were 1.6 mM, 0.86 mM, 0.56 mM and 0 mM, in the order of increasing T1 value. The parameters for the gold-standard IR sequence were as follows: Single-shot gradient echo EPI with matrix size = 128×128, FOV = 200mm × 200mm, leading to 1.56mm × 1.56mm in-plane resolution. Slice thickness = 2mm, TE = 19 ms, Bandwidth = 1562 Hz/pixel, GRAPPA R = 2, Number of calibration lines = 30, Partial Fourier Factor = 6/8. (The parameters up to this point were the same for TOWERS.) TR > 20 sec in order to ensure full recovery after each measurement, Number of slices = 1, # TI values = 42 with an additional, almost fully relaxed M_o scan at the very beginning, Minimum TI value = 25 ms, Maximum TI value = 14525 ms. The total acquisition time was about 21 minutes.

As for TOWERS: TR = 4000 ms for all repetitions including GRAPPA calibrations, SR repetitions and IR repetitions, Number of slices = 60, Number of repetitions = 33 that include three saturation recovery (SR) samples – one at the beginning, one in the middle and one at the end. Slice 30 was matched with the single-slice gold standard acquisition above. The total acquisition time was 2 minutes and 32 seconds.

In order to test the performance in vivo, data was collected from four subjects with ages between 22 and 36 years. The study was conducted in accordance with the regulations of the Institutional Review Board (IRB).

For each of the first three subjects, 4 data sets were collected with no motion to observe the reproducibility of TOWERS and 1 data set was collected with motion where the subject was asked to move twice – once within Acquisition Period 1 and once within Acquisition Period 2. The fourth, highly-motivated subject was able to turn his head by more than 90 degrees inside the MR scanner and his data set was used to demonstrate the value of GRAPPA recalibration.

In addition to the TOWERS scans, the single-slice IR sequence was also run on the first three subjects. The acquisition parameters used in vivo for both TOWERS and IR were exactly the same as those used in the phantom experiment.

Results

TOWERS vs. IR in phantom and in vivo

Figure 5 (a) depicts the Bland-Altman plot for the phantoms that mimic various anatomical regions inside the brain. The error bars show the standard deviations of the percent differences. It can be seen that TOWERS is able to yield T1 estimates that are mostly within 5% of the true values. Figure 5 (b) is the Bland-Altman plot to compare TOWERS with IR in vivo. Unlike the phantom results, the T1 values estimated by TOWERS are significantly lower than those estimated by the single-slice IR method.

T1 measurements in various anatomical regions

Figure 6 (a) exhibits a number of anatomical regions used for assessing reliability whereas Figure 6 (b) depicts the coefficients of variation (CVs) calculated as the standard deviation divided by the mean across all 4 scans for each subject. It can be seen that all of the CVs are below 1.5%, which indicates the reliability of method.

GRAPPA calibration update

Figure 7 demonstrates the importance of GRAPPA recalibration. It can be seen that retrospective reconstruction with the proper GRAPPA weight set is able to mitigate the strong ghosting caused by motion.

T1 measurements in the case of motion

Figure 8 compares the T1 maps obtained using the motion-free data and the motion-corrupted data. Figure 8 (b) shows that motion significantly damages the T1 computation even after removing the ghosting caused by GRAPPA failure, and hence suggests that magnetization tracking is critically important in measuring T1. Magnetization tracking by treating the whole voxel as a single unit leads to an improved T1 map (Figure 8 (c)) when compared to the case with no tracking (Figure 8 (b)). However, some of the voxels on the same slice are relocated onto different slices after motion, which leads to noticeable roughness and bright spots in the image. After considering the voxels as a lattice of spin volumes using either a 3×3×3 grid or a 5×5×5 grid, the roughness and the bright spots are mostly eliminated as seen in Figure 8 (d) and (e). The T1 values listed in the figure indicate the quantitative success of the magnetization tracking scheme. It is worth noting that the results for the 3×3×3 ($N_{SVsPerDim}$=3) and the 5×5×5 ($N_{SVsPerDim}$=5) grids are almost identical. This is a case of diminishing returns because, as $N_{SVsPerDim}$ is increased, the computation time increases substantially.

Table 1 shows the results across three subjects (i) in the absence of motion, (ii) in the presence of motion, but with no magnetization tracking and (iii) in the presence of motion, but with sub-voxel magnetization tracking ($N_{SVsPerDim}$=3). It can be seen that the results

obtained via sub-voxel magnetization tracking using the motion-corrupted data are comparable to those obtained using the motion-free data.

Efficiency comparison

Table 2 lists the efficiency of the gold-standard IR method, Clare and Jezzard's method (19), Zhu and Penn's method (20) and TOWERS. It can be seen that TOWERS is by far the most efficient sequence among the four listed here.

Discussion

We improve upon the existing slice reordering methods in several aspects: (i) A high number of samples can be collected in a very short time. In terms of the metric defined in Eq. [1], TOWERS is the most efficient among the slice reordering methods proposed to date. More specifically, the method proposed in (19) used a 15-second idle time for each sub-volume block in order to achieve full recovery, which reduces the scan efficiency. On the other hand, the method in (20) used a multi-shot acquisition, which trades time for image quality and is thus time-inefficient. (ii) Multiple GRAPPA calibration scans are acquired. This way, each repetition can be reconstructed retrospectively with the most appropriate set of coefficients in the case of motion, which alleviates ghosting in the images. (iii) Three saturation recovery (SR) samples are utilized for estimating the motion parameters through rigid registration. (iv) The motion parameters estimated via the registration of the SR samples are used to perform sub-voxel magnetization tracking and this makes it possible to produce T1 maps even in the presence of severe motion. This makes TOWERS robust. To the best of our knowledge, the effects of motion are being incorporated into the estimation procedure for the first time in the T1 mapping literature.

TOWERS can yield highly accurate T1 maps in phantom – good agreement was observed with the gold-standard IR sequence. However, the T1 values measured in normal subjects using TOWERS are lower than those obtained by the single-slice IR method. We investigated several plausible reasons for this underestimation, including interslice cross-talk, inversion profile effects, short TR effects, perfusion effects and magnetization transfer effects. Based on the additional experimental results not shown in this paper, the first three factors were found to have only a marginal impact on the underestimation. Perfusion seems to be the main factor. This is supported by the significantly lower underestimation in CSF compared to the other anatomical regions because the T1 estimation in CSF is affected by flow effects, but not by perfusion. In the single-slice IR experiment, TR is set to an extremely long value. Therefore, the perfusion-born interference from the spins outside the slice of interest is reset by the beginning of each repetition. However, for TOWERS, which is a multi-slice acquisition, perfusion leads to an exchange of spins between the imaging slice and the neighboring slices, within which the spins are at different stages of T1 recovery. As suggested previously (20,25), the measured T1 value is, due to perfusion, an apparent T1 value, which is smaller than the true T1 value. Magnetization transfer effects do not exist in phantom, but they do exist in human studies. The exchange of bound protons and free protons may have an impact on T1 estimation. However, controversial results have been reported in the literature (26,27).

We also compared our results to the previously published methods. It is worth noting that the in vivo T1 values for the human brain reported to date are already quite diverse. For instance, the T1 value for the frontal white matter was found to be 699±38 ms in (28), 761±25 ms in (20), 838±38 ms in (29) and 847±43 ms in (30). In this study, it was measured to be 687±21 ms. Thus far, the factors leading to the diverse in vivo results in the literature have yet to be thoroughly discovered. Nevertheless, the method proposed in this study is able to yield highly reproducible results, making it a reliable method for clinical use.

In this study, we did not assume a perfect B1 field for the inversion and excitation RF pulses. Instead, the actual flip angles were treated as additional unknown parameters during fitting. By doing so, the number of fitted parameters increased from 2 to 4. This four-parameter approach makes T1 estimation less sensitive to B1 inhomogeneity. However, with this four-parameter approach, the statistical power is reduced and the computation time is lengthened. In this respect, for clinical applications where the accuracy of the T1 values is not extremely critical and a map with apparent T1 values is sufficient, the two-parameter fitting can be utilized as a quick alternative. For example, we have observed that, compared to the commonly used T1 MPRAGE sequence, the deep gray structures such as the putamen and the caudate are better delineated with our T1 maps, even when only 2 parameters are fitted.

Our study has a few limitations. Although the phantom study demonstrated a good agreement between TOWERS and the gold standard IR sequence, the in vivo study shows that the T1 values measured by TOWERS in the human brain are lower than those measured by the single-slice IR method. As mentioned above, tissue perfusion is the most likely reason to explain this discrepancy. Therefore, the T1 value obtained by TOWERS should be considered as apparent T1. Another limitation is that, if motion is severe with large through-plane motion, our 3×3×3 sub-voxel magnetization tracking may not be adequate to completely remove the motion artifacts in the T1 maps. In this case, a 5×5×5 or finer sub-voxel magnetization tracking is advisable.

In EPI sequences, the sampling bandwidth along the phase encoding axis is usually low and it may lead to local geometric distortion. If the subject rotates his head by 45 degrees, phase encoding will now take place along an axis that is 45 degrees away from the original axis, which, in turn, changes the direction along which geometric distortion will occur. The change of geometric distortion direction in a local region leads to relocation of some voxels and causes signal intensity changes, which might eventually impact the estimated T1 values. Under this situation, it is challenging to completely correct the effects of motion using a retrospective method. To address this issue, a prospective acquisition correction scheme can be employed in the future. After detecting and estimating motion, the acquisition frame of reference should follow the subject and keep the phase encoding direction the same.

In summary, we have developed a highly efficient and robust method for T1 measurement in phantom and in vivo. Future work includes a demonstration of its clinical utility in various neurological diseases during which T1 values are altered.

Conclusions

The proposed method, TOWERS, provides a very efficient imaging scheme for T1 mapping. Accurate and highly repeatable T1 measurements are achieved. The update of the GRAPPA coefficients and the tracking of the sub-voxel magnetization make the proposed method robust to motion.

Acknowledgements

This work is supported in part by NIH 1R01NS082561 and R01NS055754.

References

1. Tofts PS. Modeling tracer kinetics in dynamic Gd-DTPA MR imaging. J Magn Reson Imaging. 1997; 7:91–101. [PubMed: 9039598]
2. Bergamino M, Saitta L, Barletta L, Bonzano L, Mancardi GL, Castellan L, Ravetti JL, Roccatagliata L. Measurement of blood-brain barrier permeability with T1-weighted dynamic contrast-enhanced MRI in brain tumors: a comparative study with two different algorithms. ISRN Neurosci. 2013; 2013:6.
3. Larsson HB, Courivaud F, Rostrup E, Hansen AE. Measurement of brain perfusion, blood volume, and blood-brain barrier permeability, using dynamic contrast-enhanced T1-weighted MRI at 3 tesla. Magn Reson Med. 2009; 62:1270–1281. [PubMed: 19780145]
4. Wang J, Alsop DC, Li L, Listerud J, Gonzalez-At JB, Schnall MD, Detre JA. Comparison of quantitative perfusion imaging using arterial spin labeling at 1.5 and 4.0 Tesla. Magn Reson Med. 2002; 48:242–254. [PubMed: 12210932]
5. Xu G, Rowley HA, Wu G, Alsop DC, Shankaranarayanan A, Dowling M, Christian BT, Oakes TR, Johnson SC. Reliability and precision of pseudo-continuous arterial spin labeling perfusion MRI on 3.0 T and comparison with 15O-water PET in elderly subjects at risk for Alzheimer's disease. Nmr Biomed. 2010; 23:286–293. [PubMed: 19953503]
6. Parker DL, Smith V, Sheldon P, Crooks LE, Fussell L. Temperature distribution measurements in two-dimensional NMR imaging. Med Phys. 1983; 10:321–325. [PubMed: 6877179]
7. Dickinson RJ, Hall AS, Hind AJ, Young IR. Measurement of changes in tissue temperature using MR imaging. J Comput Assist Tomogr. 1986; 10:468–472. [PubMed: 3700752]
8. Peller M, Reinl HM, Weigel A, Meininger M, Issels RD, Reiser M. T1 relaxation time at 0.2 Tesla for monitoring regional hyperthermia: feasibility study in muscle and adipose tissue. Magn Reson Med. 2002; 47:1194–1201. [PubMed: 12111966]
9. Fleckenstein JL, Archer BT, Barker BA, Vaughan JT, Parkey RW, Peshock RM. Fast short-tau inversion-recovery MR imaging. Radiology. 1991; 179:499–504. [PubMed: 2014300]
10. De Coene B, Hajnal JV, Gatehouse P, Longmore DB, White SJ, Oatridge A, Pennock JM, Young IR, Bydder GM. MR of the brain using fluid-attenuated inversion recovery (FLAIR) pulse sequences. AJNR Am J Neuroradiol. 1992; 13:1555–1564. [PubMed: 1332459]
11. Carr HY, Purcell EM. Effects of Diffusion on Free Precession in Nuclear Magnetic Resonance Experiments. Phys Rev. 1954; 94:630–638.
12. Freeman R, Hill HDW. Fourier transform study of NMR spin-lattice relaxation by progressive saturation. J Chem Phys. 1971; 54:3367–3377.
13. Fram EK, Herfkens RJ, Johnson GA, Glover GH, Karis JP, Shimakawa A, Perkins TG, Pelc NJ. Rapid calculation of T1 using variable flip angle gradient refocused imaging. Magn Reson Imaging. 1987; 5:201–208. [PubMed: 3626789]
14. Look DC, Locker DR. Time saving in measurement of NMR and EPR relaxation times. Rev Sci Instrum. 1970; 41:250–251.
15. Graumann R, Barfuss H, Fischer H, Hentschel D, Oppelt A. TOMROP: a sequence for determining the longitudinal relaxation time in magnetic resonance tomography. Electromedica. 1987; 55:67–72.

16. Gowland PA, Leach MO. Fast and accurate measurements of T1 using a multi-readout single inversion-recovery sequence. Magn Reson Med. 1992; 26:79–88. [PubMed: 1625570]
17. Shin W, Gu H, Yang Y. Fast high-resolution T1 mapping using inversion-recovery look-locker echo-planar imaging at steady state: Optimization for accuracy and reliability. Magn Reson Med. 2009; 61:899–906. [PubMed: 19195021]
18. Ordidge RJ, Gibbs P, Chapman B, Stehling MK, Mansfield P. High-speed multislice T1 mapping using inversion-recovery echo-planar imaging. Magn Reson Med. 1990; 16:238–245. [PubMed: 2266843]
19. Clare S, Jezzard P. Rapid T1 mapping using multislice echo planar imaging. Magn Reson Med. 2001; 45:630–634. [PubMed: 11283991]
20. Zhu DC, Penn RD. Full-brain T1 mapping through inversion recovery fast spin echo imaging with time-efficient slice ordering. Magn Reson Med. 2005; 54:725–731. [PubMed: 16086307]
21. Eldeniz C, Lin W, An H. TOWERS: T-One With Enhanced Robustness and Speed. In Proceedings of the 21st Annual Meeting of the ISMRM. 2013:4212.
22. Griswold MA, Jakob PM, Heidemann RM, Nittka M, Jellus V, Wang J, Kiefer B, Haase A. Generalized autocalibrating partially parallel acquisitions (GRAPPA). Magn Reson Med. 2002; 47:1202–1210. [PubMed: 12111967]
23. Jenkinson M, Smith S. A global optimisation method for robust affine registration of brain images. Med Image Anal. 2001; 5:143–156. [PubMed: 11516708]
24. Jenkinson M, Bannister P, Brady M, Smith S. Improved optimization for the robust and accurate linear registration and motion correction of brain images. Neuroimage. 2002; 17:825–841. [PubMed: 12377157]
25. Detre JA, Leigh JS, Williams DS, Koretsky AP. Perfusion Imaging. Magnetic Resonance in Medicine. 1992; 23:37–45. [PubMed: 1734182]
26. Robson MD, Piechnik SK, Tunnicliffe EM, Neubauer S. T-1 measurements in the human myocardium: The effects of magnetization transfer on the SASHA and MOLLI sequences. Magnetic Resonance in Medicine. 2013; 70:664–670. [PubMed: 23857710]
27. Ehses P, Seiberlich N, Ma D, Breuer FA, Jakob PM, Griswold MA, Gulani V. IR TrueFISP with a golden-ratio-based radial readout: Fast quantification of T-1, T-2, and proton density. Magnetic Resonance in Medicine. 2013; 69:71–81. [PubMed: 22378141]
28. Lu H, Nagae-Poetscher LM, Golay X, Lin D, Pomper M, van Zijl PC. Routine clinical brain MRI sequences for use at 3.0 Tesla. J Magn Reson Imaging. 2005; 22:13–22. [PubMed: 15971174]
29. Wansapura JP, Holland SK, Dunn RS, Ball WS Jr. NMR relaxation times in the human brain at 3.0 tesla. J Magn Reson Imaging. 1999; 9:531–538. [PubMed: 10232510]
30. Gelman N, Ewing JR, Gorell JM, Spickler EM, Solomon EG. Interregional variation of longitudinal relaxation rates in human brain at 3.0 T: relation to estimated iron and water contents. Magn Reson Med. 2001; 45:71–79. [PubMed: 11146488]

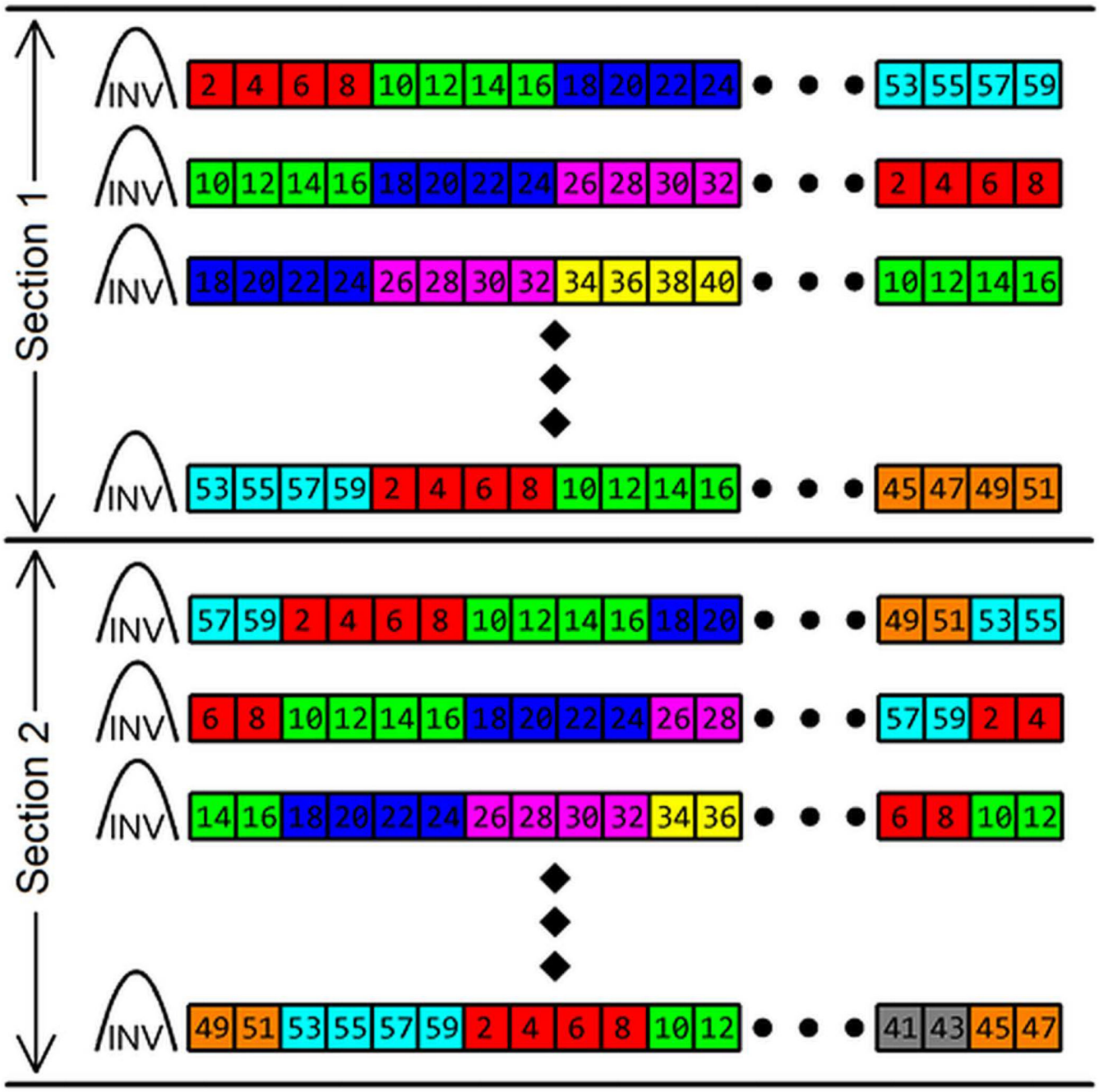

Figure 1.
Slice reordering scheme for a 60-slice acquisition

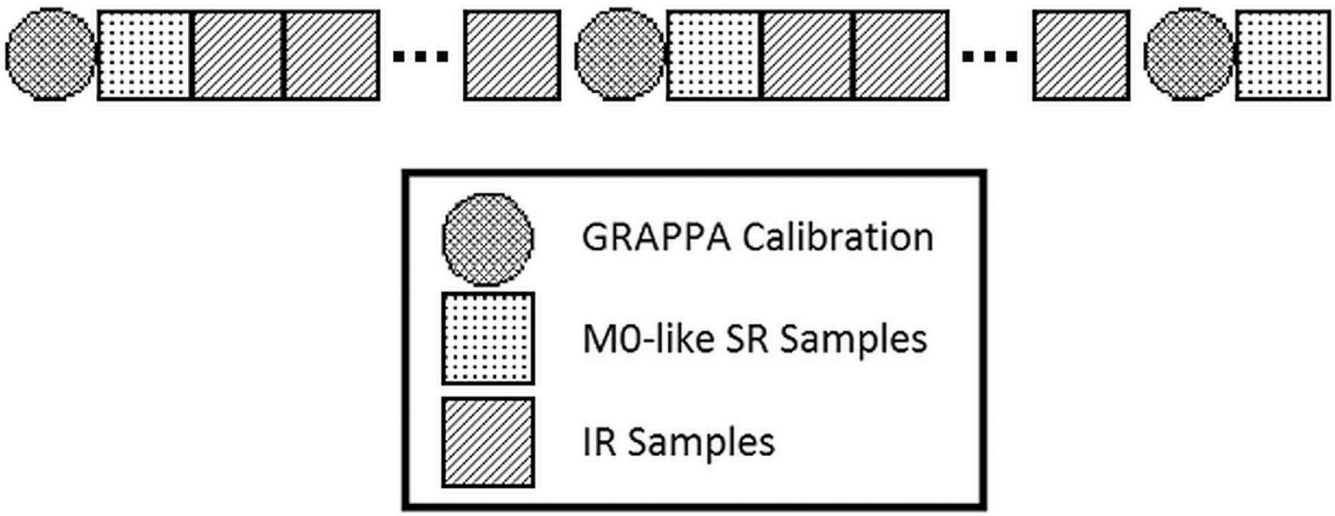

Figure 2.
Overall acquisition scheme

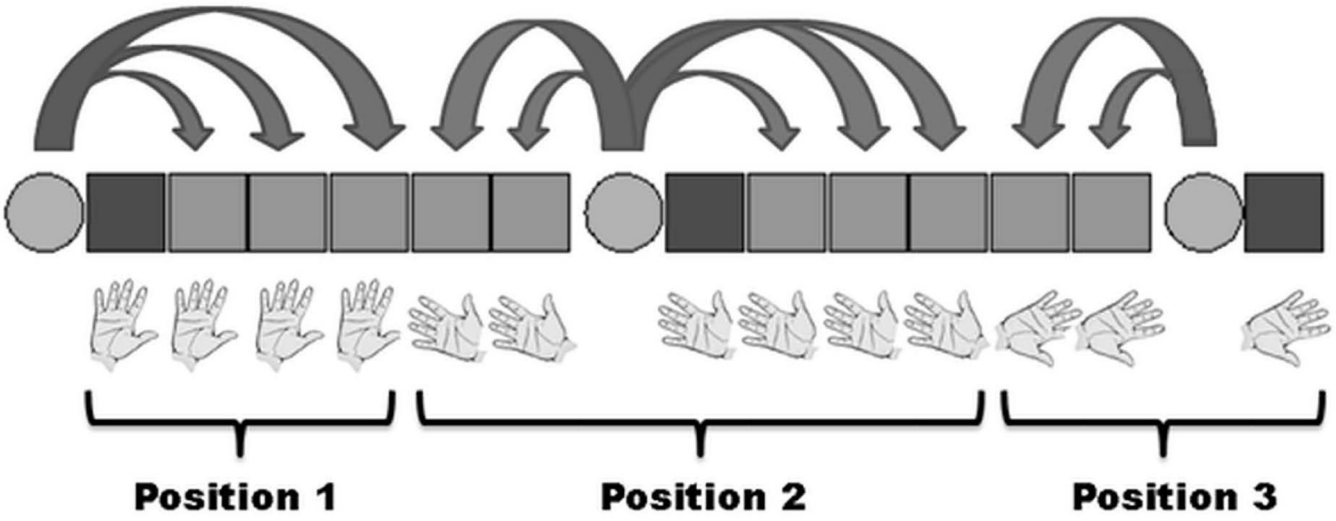

Figure 3.

Retrospective reconstruction in the presence of motion. Arrows show to which IR repetitions a given set of calibration data is applied. Hands represent the High5 slices. The change of position is indicated by the change in the orientation of the hands.

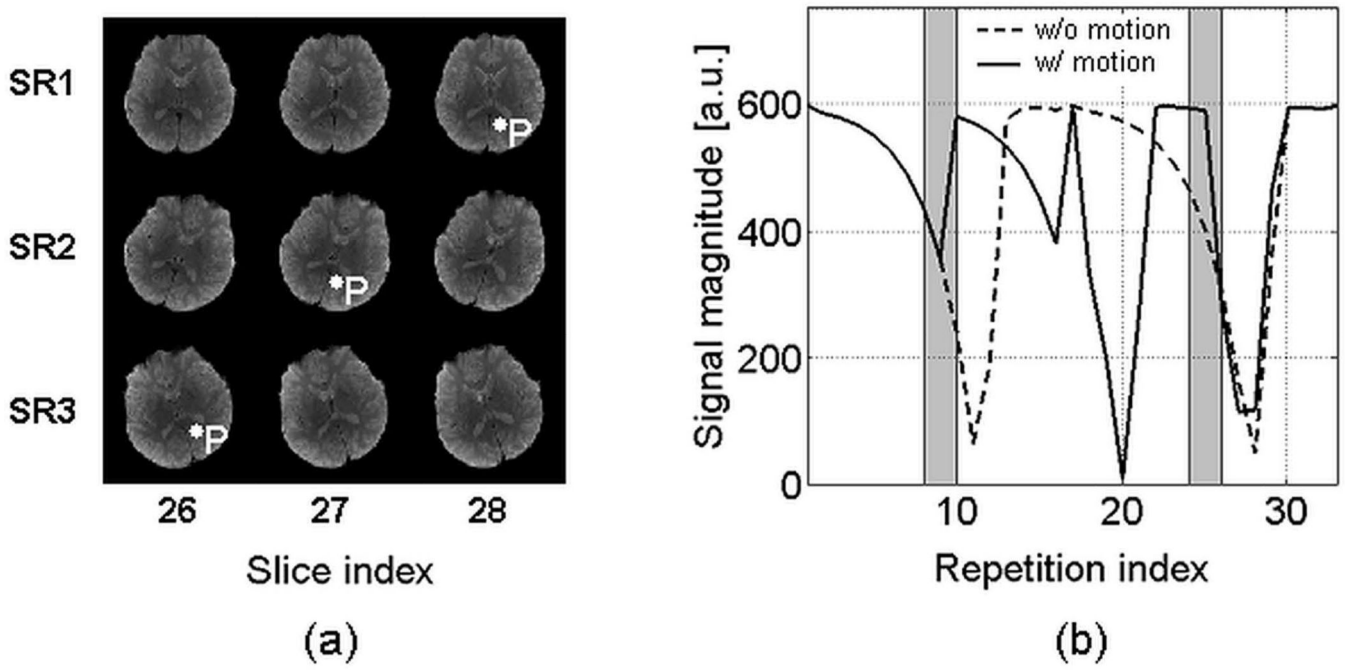

Figure 4.

(a) Three adjacent slices from the three SR repetitions. The subject moved in each of the two acquisition periods of the sequence. P represents a voxel that gets relocated onto a different slice because of motion. (b) Motion-free and motion-corrupted magnetization pathways for the spins that belong to Voxel P shown in (a). The gray bands indicate the instances of motion.

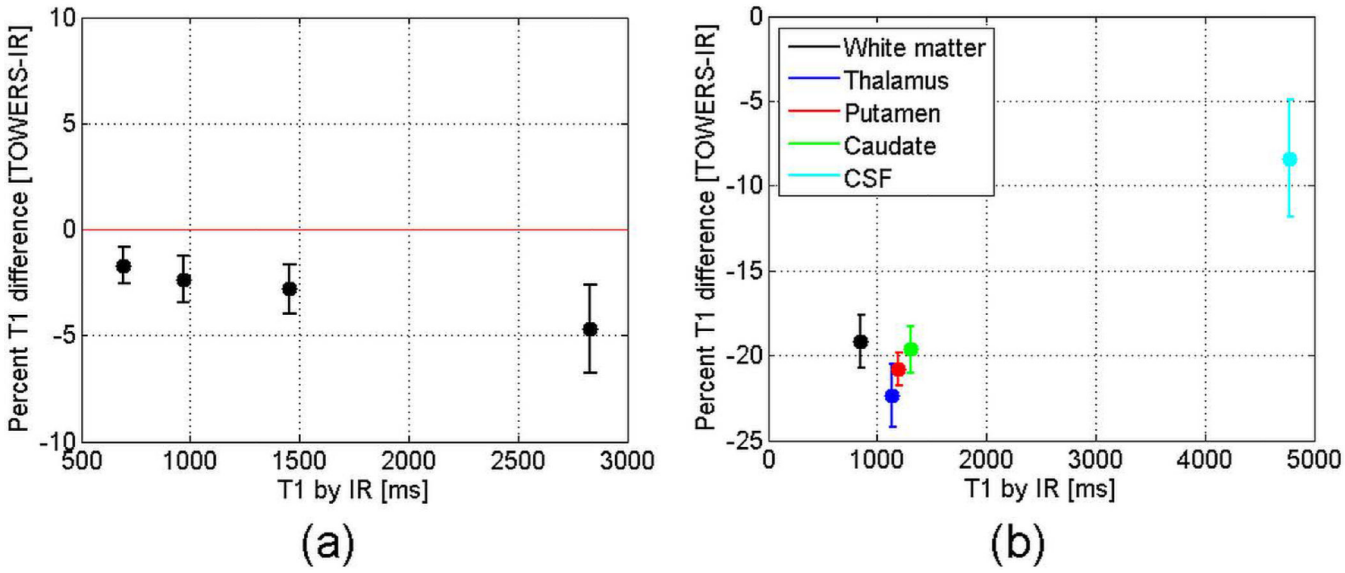

Figure 5.

Bland-Altman plot demonstrating the percent T1 difference between TOWERS and IR as a function of the T1 values yielded by IR (a) in phantom and (b) in vivo. The approximate concentrations of the phantoms were 1.6 mM, 0.86 mM, 0.56 mM and 0 mM, in the order of increasing T1 value. The length of the error bars is 1 standard deviation.

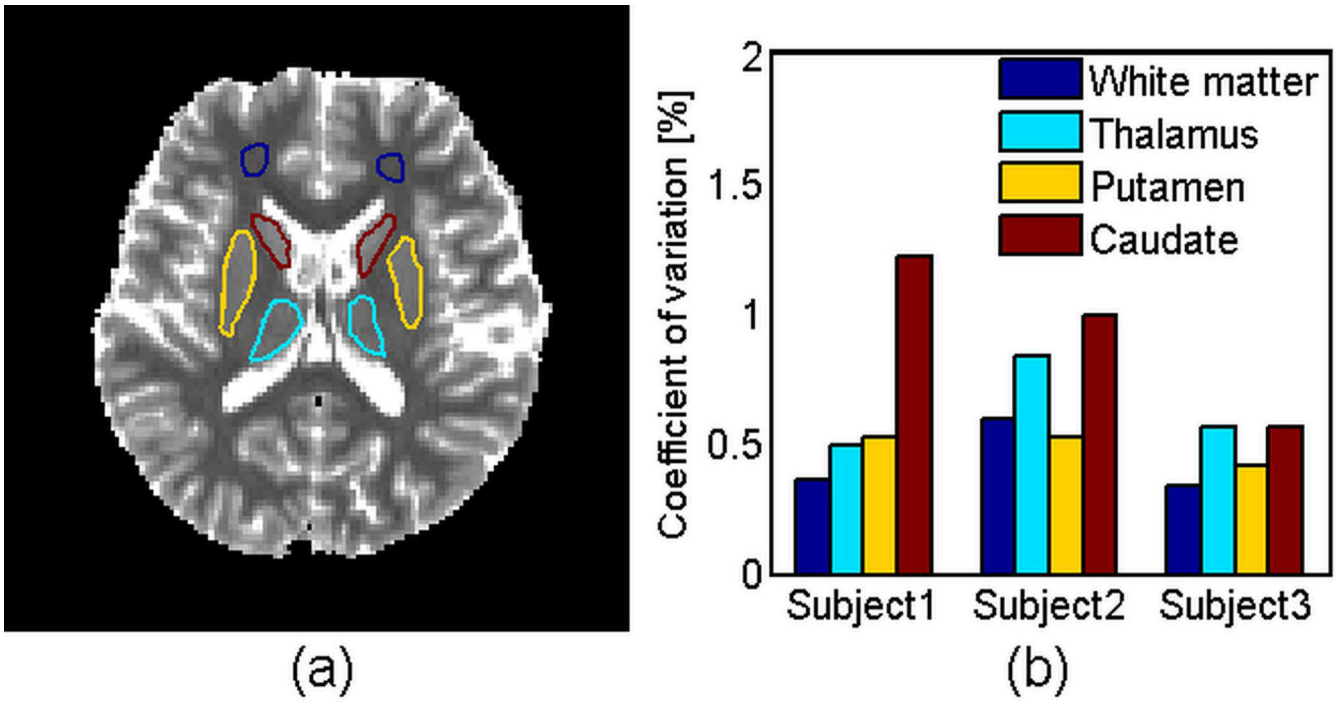

Figure 6.

(a) – Anatomical regions of interest: Frontal white matter (blue outline), thalamus (cyan outline), putamen (yellow outline) and caudate (red outline) (b) Coefficients of variation across four identical scans

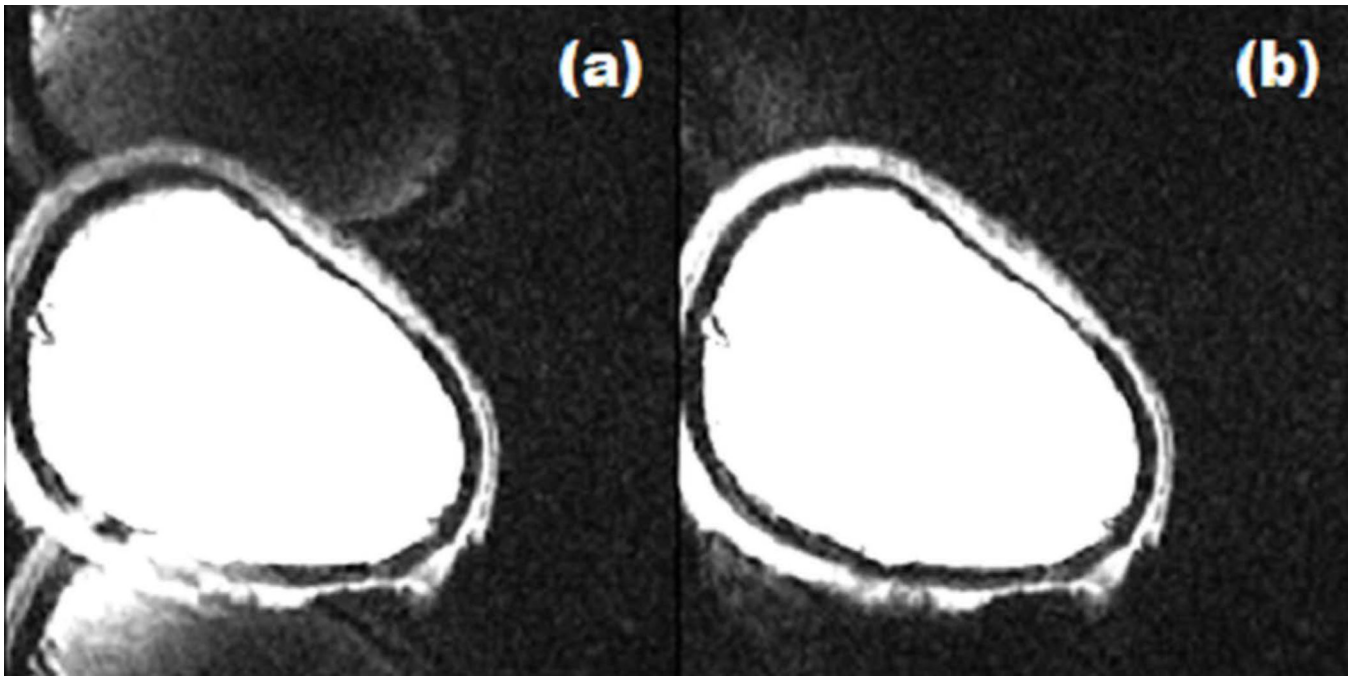

Figure 7.
Image reconstructed with (a) improper, (b) proper GRAPPA calibration. The window level was adjusted to emphasize the ghosting around the image.

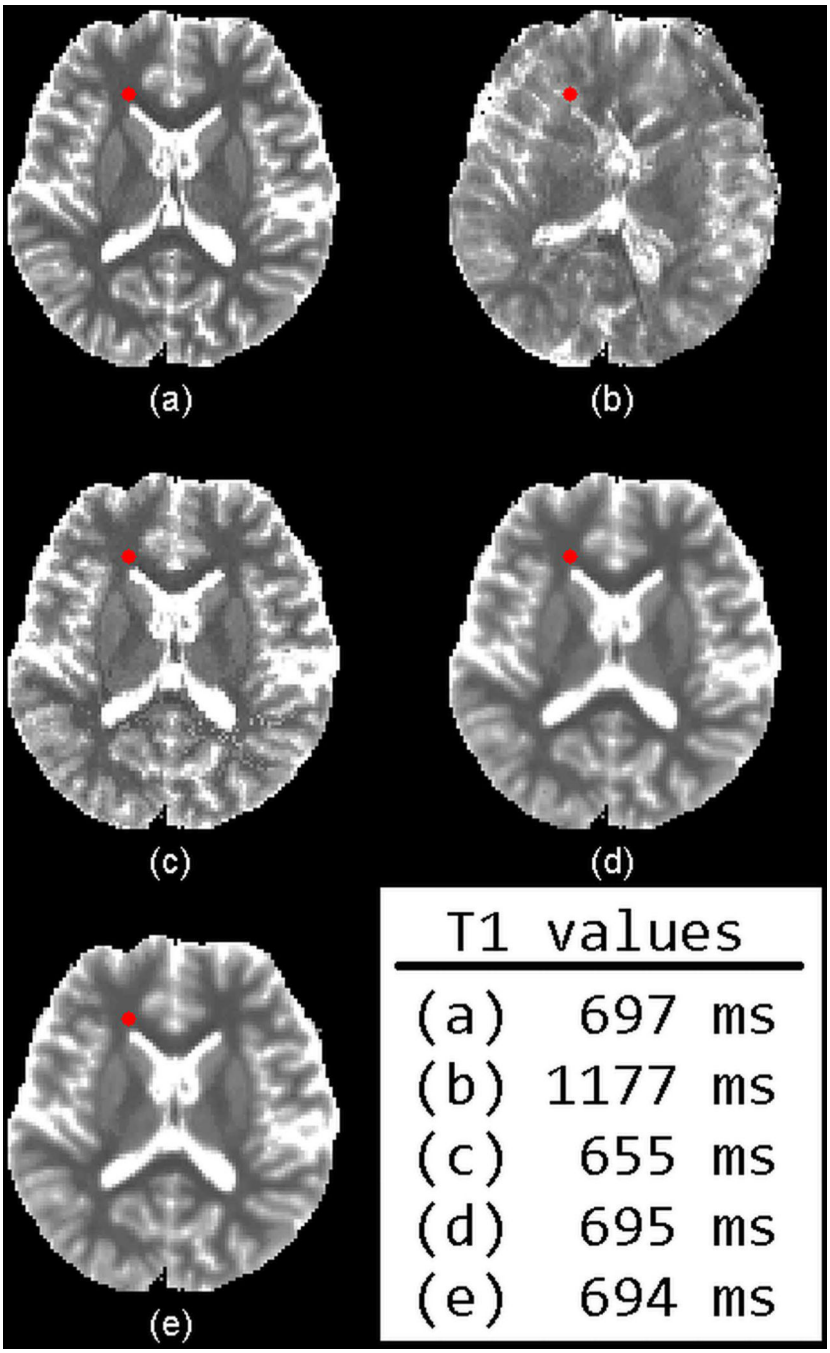

Figure 8.

(a) Motion-free, (b) Motion-corrupted processed with no magnetization tracking, (c–e) Motion-corrupted processed with magnetization tracking where $N_{SVsPerDim}$=1, $N_{SVsPerDim}$=3 and $N_{SVsPerDim}$=5, respectively. The T1 values are for the voxel marked with the open white circles.

Table 1

T1 values (mean±std in ms) across three subjects for various anatomical regions

	Motion-free	Motion-corrupted	Motion-corrected
White matter	687±21	933±30	695±40
Putamen	947±18	918±54	953±20
Thalamus	884±28	1070±186	892±20
Caudate	1046±25	914±108	1037±36
CSF	4359±15	1176±106	4003±280

Table 2

Efficiency comparison

	# Slices	# Data points	Total acquisition time	η
Inversion recovery	1	43	21 min	0.03
Clare & Jezzard	60	12	3 min	4
Zhu & Penn	12	6	6 min 32 sec	0.18
TOWERS	60	33	2 min 32 sec	13.03